Fire Safety Journal 139 (2023) 103829

Contents lists available at ScienceDirect

Fire Safety Journal

journal homepage: www.elsevier.com/locate/firesaf

Analysis of combustion gases from large-scale electric vehicle fire tests

Jonna Hynynen [a,*], Ola Willstrand [a], Per Blomqvist [a], Petra Andersson [b]

[a] Research Institutes of Sweden RISE, Department of Fire and Safety, Brinellgatan 4, 50462, Borås, Sweden
[b] Lund University, Division of Fire Safety Engineering, John Ericssons väg 1, 22363, Lund, Sweden

ARTICLE INFO

Keywords:
Combustion gas
Heat release rate
Electric vehicle
Large-scale fire test
Lithium-ion battery

ABSTRACT

Fires involving electric vehicles have attracted considerable attention in the media. In particular, the toxic gases released upon combustion of electric vehicles and lithium-ion batteries has been a major concern. In this study, the results of six large-scale vehicle fire tests are presented including three electric vehicles, two internal combustion engine vehicles, and one electric vehicle with the battery pack removed. Additionally, separate battery component tests were performed. In two of the vehicle fire tests a sprinkler system was used to assess the effect of water application on the combustion gases. Furthermore, calculations of the heat release rate, peak heat release rate and total heat release were performed, as well as chemical analysis of gas and soot. Peak heat release rate and total heat release were affected by the fire scenario and vehicle model, but not significantly by the type of powertrain. Regarding the combustion gases, hydrogen fluoride represented the largest difference between electric vehicles and internal combustion engine vehicles. Additionally, battery specific metals such as manganese, nickel, cobalt and lithium were found in higher concentrations in the electric vehicle tests than in the internal combustion vehicle tests, in which larger quantities of lead were found.

1. Introduction

Fire incidents that involve electric vehicles (EVs) have attracted considerable attention in the media during the past years [1,2]. Furthermore, increased fire risks related to lithium-ion batteries (LIBs) are often pointed out, even though most fire incidents involving EVs have fire origins other than the traction battery. The currently available statistics support the claim that EV fires are less probable than internal combustion engine vehicle (ICEV) fires [1,3,4]. Nevertheless, unexpected mechanical or thermal loading or internal failures in the LIB can lead to thermal runaway [1]. Thermal runaway is a state of rapid self-heating, driven by exothermic chemical reactions inside the battery cell/s which can lead to a fire.

For LIB fires, the emission of hydrogen fluoride (HF) has sparked a major concern. The origin of HF in LIB fires can be attributed to the combustion of the electrolyte. The electrolyte contains lithiated salts such as, lithium hexafluorophosphate ($LiPF_6$), as well as other fluorine containing compounds [5] which provide the possibility for HF emissions during heating and combustion. HF can also be formed upon combustion of the air conditioner coolant or from the combustion of highly fluorinated polymers such as polyvinylidene fluoride (PVDF) [6,7].

The potential dangers of HF have naturally triggered a huge concern with the public. Since the early reports on HF emissions from LIB fires, many studies have been performed to thoroughly investigate possible hazards. For example, Wingfors et al. [8] studied the protection factor for standard firefighter protective clothing (also known as bunker gear or turnout gear) towards HF, as well as the dermal uptake of gaseous HF. The protection factor of the tested firefighting clothing was on average 120, meaning that the concentration of HF was 120 times lower on the inside of the clothing than on the outside. Furthermore, the study concluded that adverse health effects caused by skin exposure to HF during firefighting is very unlikely. Additionally, Dennerlein et al. [9] studied the dermal penetration of HF in solution. It was found that upon a 24 h exposure to HF (5–30 wt%), only a small amount (~1%) was able to penetrate the skin. Increasing the HF concentration to 50 wt% leads to a skin penetration of 8%. Furthermore, using data from Dennerlein et al. [9] and Wingfors et al. [8], the ambulance service in Stockholm (AISAB), estimated that a deadly dose of HF through inhalation, would require an exposure of 100 ppm for ~ 2–12 h (assuming heavy breathing of 2400 L h^{-1}) [10].

The reported concentrations of HF upon combustion of vehicles and

* Corresponding author.
E-mail addresses: jonna.hynynen@ri.se (J. Hynynen), ola.willstrand@ri.se (O. Willstrand), per.blomqvist@ri.se (P. Blomqvist), petra.andersson@ri.se (P. Andersson).

https://doi.org/10.1016/j.firesaf.2023.103829
Received 22 March 2023; Received in revised form 27 April 2023; Accepted 24 May 2023
Available online 25 May 2023

LIBs vary to a large extent. In several studies attempts have been made to extrapolate emissions from single LIB cells to larger battery systems (including vehicles) [11–16]. For example, in work by Larsson et al. [11], it was estimated that 20–200 mg W^{-1} h^{-1} of HF could be released from a battery fire. In work by Willstrand et al. [17], a comparison between different battery fire tests and HF emissions was made; the total HF emissions ranged between 1 and 250 ppm kWh^{-1} calculated for a reference volume of 1000 m^3.

Furthermore, combustion gases from all types of vehicle fires include a range of other toxic compounds, such as carbon monoxide (CO), hydrogen cyanide (HCN), hydrochloric acid (HCl) and polycyclic aromatic hydrocarbons (PAHs). Asphyxiant gases, such as CO and HCN, may cause unconsciousness or death by asphyxia. In a study by Viklund et al. [18], the cause of death in fatal car crashes was investigated. In 55 of the cases (30%), the cause of death could be related to burns and/or smoke inhalation.

Particulate-bound compounds, such as inorganics and PAHs, are found in all vehicle fires. In work by Mellert et al. [19], it was found that metals associated with particulates from EV fires had high levels of cobalt, lithium and manganese. In work by Lönnermark and Blomqvist [20], particulate-bound metals found in ICEV fires were analysed and high concentrations of zinc, lead and copper were found. Ambient particulate matter is a serious health issue and epidemiological studies have associated several acute health effects to the inhalation of particulate matter [21–23]. PAHs are persistent and cancerogenic and are a known health risk for firefighters [24–27].

The total quantities of toxic emissions have previously been reported by many researchers, for example, in Ref. [28] for EV fire tests; in Refs. [11,12,29–32] for LIBs and in Refs. [20,33] for ICEVs. A comparison of the concentration of different gases (per vehicle or per Wh) to various health exposure limit values (from The National Institute for Occupational Safety and Health, United States Environmental Protection Agency, and The Swedish Work Environment Authority) indicates that CO and HCN were found in quantities higher than their health exposure limits.

Only a limited number of large-scale fire tests on EVs can be found in literature, which are presented in Refs. [28,34–36]. Moreover, studies on asphyxiant or irritant gases, such as HCN, HCl or HF from EV fires are even more limited. Hence, more research is needed to provide experimentally validated data to better understand the hazard associated with EV fires. The data sets reported within this work could for example be used to assess current (or future engineering of) fire protection system designs or/and to assess the environmental and human health impact of vehicle fires. In work by Lecocq et al. [28], combustion gases from both ICEVs and EVs were studied; it was highlighted that the total concentrations of CO_2, CO, total hydrocarbons, NO, NO_2, HCl and HCN were similar for both types of vehicles. In this work, the results from six large-scale vehicle fire tests as well as from several battery components (cell/module/pack) fire tests are reported. Heat release rates (HRR), total heat release (THR) and chemical analysis of the combustion gases are presented. Additionally, application of water using a sprinkler system was performed to determine the contamination of extinguishing water, which is published elsewhere [37].

2. Materials and methods

2.1. Test setup

Six large-scale vehicle fire tests were performed. For safety reasons, some modifications of the vehicles were necessary. These modifications included puncturing the tires and disabling dampers and suspensions. Additionally, the windows were closed at the start of each test. The specifications of the vehicles, ignition sources and if a sprinkler system was active during the test are presented in Table 1. The sprinkler system used in these tests is described in the Supplementary Material section S1.1.

Tests 4–6, presented in Table 1, were performed in 2020 and have previously been published in a technical report [17]. Test results are included in this work for comparison with the more recent tests performed in 2022 (Table 1, tests 1–3).

All tests were performed inside a fire hall equipped with a large calorimeter hood (Ø = 6 m) to enable collection of smoke and gas emissions. Advanced flue gas reduction and water purification systems are linked to the fire hall to minimise exhausts to the environment. An overview of the test setup is illustrated in Fig. 1. The ignition source was selected to create a worst-case scenario and to involve the traction energy early in the fire (see Table 1 for ignition sources). For safety reasons, the propane burner used for ignition (except test 4) was kept active for the complete test duration. The heat release contribution from the burner was subtracted from the vehicle fire test measurements. In test 4, no extra fuel was added; the pool fire was created using half of the fuel in the vehicle's tank.

For tests 2 and 3, a sprinkler system was activated at a HRR of 1 MW and kept active for 30 min, delivering a total of 11 160 L of water per test. After deactivation of the sprinkler system, the fire was allowed to grow again and at the end of each test the vehicles were completely burnt-out.

A large steel tray (5 × 2 × 0.15 m) was positioned under the vehicles to contain the liquid pool fire from the petrol/diesel in tests 2 and 4. In addition, in tests 2 and 3 the tray was used to collect extinguishing water, which was further analysed and results are presented in Ref. [37].

In addition to the large-scale vehicle fire tests, two battery packs were also tested. The battery components tests performed in 2020 originated from a plug-in hybrid electric SUV manufactured in 2014 and consisted of prismatic cells with a capacity rating of 40 Ah. In total, one module was used for cell-level tests, two modules were used for module-level tests, and the remaining modules were used for a "pack" test, resulting in a total of nine battery tests at different scales. The second battery pack tested in 2022 consisted of the battery pack removed from test 1. This battery pack consisted of 218 prismatic NMC cells, with a total electrical energy of 50 kWh. Application of water using a sprinkler system was employed for the full test duration in this test. However, the pack was protected from direct water impingement to avoid cooling of the battery pack. The purpose of the battery pack fire tests was to compare heat release and gas emissions from batteries in small, medium and large-scale battery components tests as well as to study the effect of water on the combustion gases.

Table 1
Specifications of the tested vehicles.

Test	Type	Traction energy	Cell type	Ignition source	Model	Year	Man.[a]	Sprinkler system
1	REF[b]	Removed[b]	–	30 kW burner	Small SUV	2021	A	N
2	ICEV	Petrol, 40 L	–	30 kW burner	Small SUV	2021	A	Y
3	EV	50 kWh, 90% SOC	NMC, prismatic	30 kW burner	Small SUV	2021	A	Y
4	ICEV	Diesel, 44 L	–	Pool fire	Full-size van	2011	B	N
5	EV	40 kWh, 80% SOC	NMC, pouch	30 kW burner	Full-size van	2019	B	N
6	EV	24 kWh, 80% SOC	NMC, prismatic	30 kW burner	Small car	2016	C	N

Tests 1–3 were performed in 2022 and tests 4–6 were performed in 2020 [17].

[a] Vehicle manufacturer.

[b] REF – Indicates an EV where the traction battery was removed and is used as a reference for test 2 and 3.

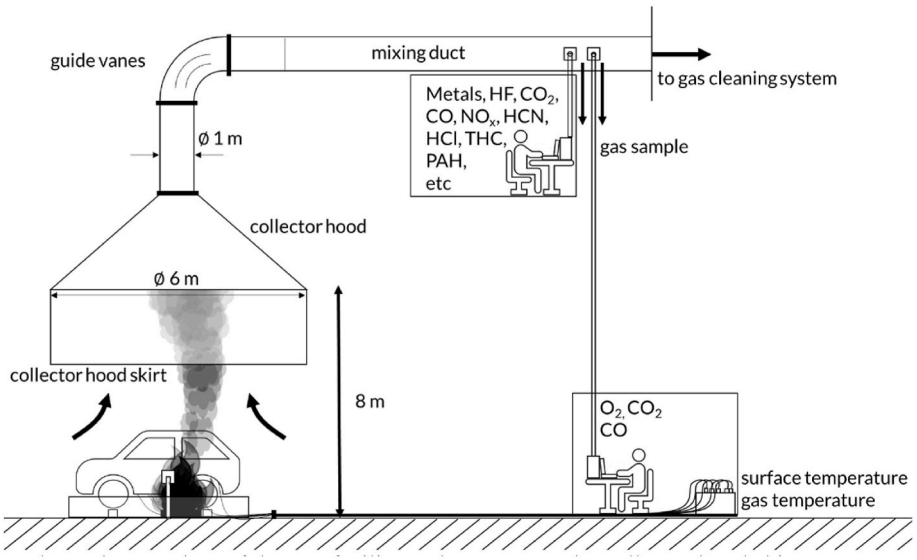

Fig. 1. Schematic overview of the test facility and test setup. The collector hood skirt was not used for tests 1–3. This schematic is reprinted with permission from Ref. [17].

2.2. Heat release rate and temperature

The mass flow rate and the concentrations of O_2, CO and CO_2 were measured in all tests, from which the HRR could be calculated. To verify that the oxygen produced from the battery upon combustion did not have a significant effect on the calorimetry-based measurements, the convective HRR was also calculated based on temperature measurements. The method and calculations used for the total HRR and convective HRR are described in Ref. [38].

2.3. Chemical analysis

To analyse the combustion gas composition, gas and soot sampling was performed from the exhaust duct (see Fig. 1). An overview of the measurement equipment used is presented in Table 2.

2.3.1. Gas analysis

A ThermoFisher Antaris FTIR instrument with a 0.2 L heated gas cell and a spectral resolution of 0.5 cm^{-1} was used for gas analysis. Sampling was performed according to ISO 19702, using a heated ceramic particle filter and a 10 m heated PTFE sampling line, and a sampling flow rate of 3.5 L min^{-1}. The sampling equipment and cell were heated to 180 °C. The ceramic filter was dispatched to an external laboratory for analysis of fluoride, chloride and bromide using high pressure ion chromatography (HPIC).

2.3.2. Total hydrocarbon content

A SICK MAIHAK Model 3006 THC-analyser with a Flame Ionization Detector (FID) was used to analyse the total hydrocarbon content. The analyser was calibrated against propane (9000 ppm). Sampling was done using a method similar to that of the FTIR sampling, through a separate heated ceramic filter and a heated PTFE sampling line, both heated to 180 °C. Gases were extracted at a sampling flow rate of 1.0 L min^{-1}.

2.3.3. Impinger sampling

Non-filtered effluent was collected and sampled using gas-washing bottles. A carbonate buffer was used to sample water-soluble halogens. The resulting solutions were analysed using high-pressure ion chromatography (HPIC).

Table 2
Overview of the equipment used, compounds measured and their chemical formula.

Measurement method	Compounds measured	Chemical formula
Fourier-Transform Infrared spectroscopy (FTIR)	Hydrogen Fluoride	HF
	Hydrogen Chloride	HCl
	Hydrogen Bromide	HBr
	Carbon Dioxide	CO_2
	Carbon Monoxide	CO
	Hydrogen Cyanide	HCN
	Sulphur Dioxide	SO_2
	Nitrogen Dioxide	NO_2
	Nitric Oxide	NO
Flame Ionization Detector (FID)	Total Hydrocarbon Content (THCs)	–
Gas washing bottles	Fluoride	F^-
	Chloride	Cl^-
	Bromide	Br^-
Gas Chromatography-Mass Spectrometry (GC-MS)	Polycyclic Aromatic Hydrocarbons (PAHs)	–
Inductively Coupled Plasma-Mass Spectrometry (ICP-MS) and ICP-Optical Emission Spectrometry (OES)	Aluminium	Al
	Cadmium	Cd
	Lead	Pb
	Cobalt	Co
	Chromium	Cr
	Copper	Cu
	Lithium	Li
	Manganese	Mn
	Nickel	Ni
	Zinc	Zn
High Pressure Ion Chromatography (HPIC)	Fluoride	F^-
	Chloride	Cl^-
	Bromide	Br^-

2.3.4. Filter sampling

Sampling of soot particles in the exhaust duct was performed by isokinetic sampling on quartz filters. At the sampling point, the flow rate was set to 50 L min^{-1} and the sampled gas flow was divided between two identical filters. The filters were dried at ambient temperature before analysis. One of the filters was analysed for metals and water-soluble anions of fluoride, chloride and bromide, the other filter was analysed for 16 types of PAH. For the metal and anion analysis, the filter was dissolved in nitric acid (240 °C) before analysing the extract using inductively coupled plasma mass spectroscopy (ICP-MS) and optical

emission spectrometry (ICP-OES). For analysis of PAHs, the filter was extracted using toluene in an ultrasonic bath for 30 min and extracts were analysed using gas chromatography-mass spectrometry (GC-MS); 16 external standards were used (see Supplementary Material Table S1).

3. Results and discussion

3.1. Heat release rates and total heat release

The HRR was calculated using oxygen consumption calorimetry and results are presented in Fig. 2. Upon activation of the sprinkler system in test 3 (Fig. 2a, blue), the HRR rapidly declined. To avoid having the sprinkler system active without thermal runaway in the battery, it was decided to turn off the sprinkler after 10 min and allow the fire to grow again. For the second activation of the sprinkler system, the sprinkler system was active for 20 min to keep the total volume of water the same for tests 2 and 3.

Upon rupture of the fuel tank for the ICEVs (Fig. 2a and b, red), the fires developed more rapidly compared to the EVs due to the release of a large amount of chemical energy.

For the tests performed in 2020 (Fig. 2b), the difference in battery configuration and especially the cell type resulted in a large difference in the HRR. When the pouch cells in test 5 (Fig. 2b, green) experienced thermal runaway, large amounts of gas were released in a relatively short time which contributed significantly to the peak HRR. In comparison, the prismatic cells in test 6 (Fig. 2b, blue) experienced thermal runaway somewhat later and continued to release gas for a longer period compared to test 5. The gas release was irregular with a slower thermal propagation between cells, resulting in a less apparent contribution to the overall HRR as noticed in Fig. 2b. A similar slower thermal propagation was also noticed in test 3 (Fig. 2a, blue) which also involved prismatic cells.

The shape of the HRR curves is different when comparing Fig. 2a and b. The reason for this divergence is foremost due to the activation of the sprinkler system, efficiently suppressing the HRR. At the time of sprinkler activation, only the exterior parts of the vehicles were burning, and the windows were intact. For test 2, the front window ruptured at a test time of 47:49 min, subsequently involving the passenger compartment in the fire. For test 3, the back window ruptured shortly after the activation of the sprinkler system (t = 12:18 min). However, during the time that the sprinkler system was active the interior of the vehicle was not involved in the fire. For test 3, the interior of the vehicle started burning at t = 22:30 min. Moreover, for the vehicle without traction energy (Fig. 2a, black), the ignition source was below the engine compartment. The fire propagation from the engine towards the back of the vehicle was very slow, resulting in a split peak in the HRR graph. This gives a clear indication that the point of fire initiation may influence the HRR. However, it did not seem to prolong or shorten the active burn time, which was on the order of ~90 min for all tests. The total mass loss in percentage and the THR were also similar amongst the tested vehicles, as presented in Table 3.

3.1.1. THR for the battery cell, module and pack tests

The THR data from the separate battery cell/module tests are plotted together with literature data from previously performed cell/module tests found in Refs. [29,39–51]. A linear correlation between the nominal electrical energy of the battery and the THR was found and is indicated by the trendline in Fig. 3.

3.2. Chemical analysis

The total quantity and the normalized amount (in g or mg per lost g) of CO_2, CO, PAHs and THC are presented in Fig. 4., the remaining gaseous compounds (HF, HCl, HBr, SO_2, NO, NO_2 and HCN) and their normalized amounts can be found in the Supplementary Material Table S2. Additionally, the gas generation rates can be found in Supplementary Material Fig. S1 (tests 1–3) and in Ref. [17] (tests 4–6). In section 3.2.1, the PAH and THC are presented; in section 3.2.3 the analysis of particulate-bound inorganics is presented and in section 3.2.4 the total quantity of HX is presented.

3.2.1. Particulate-bound polycyclic aromatic hydrocarbons and total hydrocarbon content

For the tests performed in 2022, with an active sprinkler system, the concentration of particulate-bound PAHs for the ICEV (test 2) was

Table 3
Total mass loss and THR.

	1 - REF	2 - ICEV	3 - EV	4 - ICEV	5 - EV	6 - EV
Vehicle manufacturer	A	A	A	B	B	C
Total mass loss (kg)	240	310	330	250	250	400
Total mass loss (%)	21	26	21	19	16	26
THR (GJ)	5.0	6.1	5.7	5.9	5.2	6.7

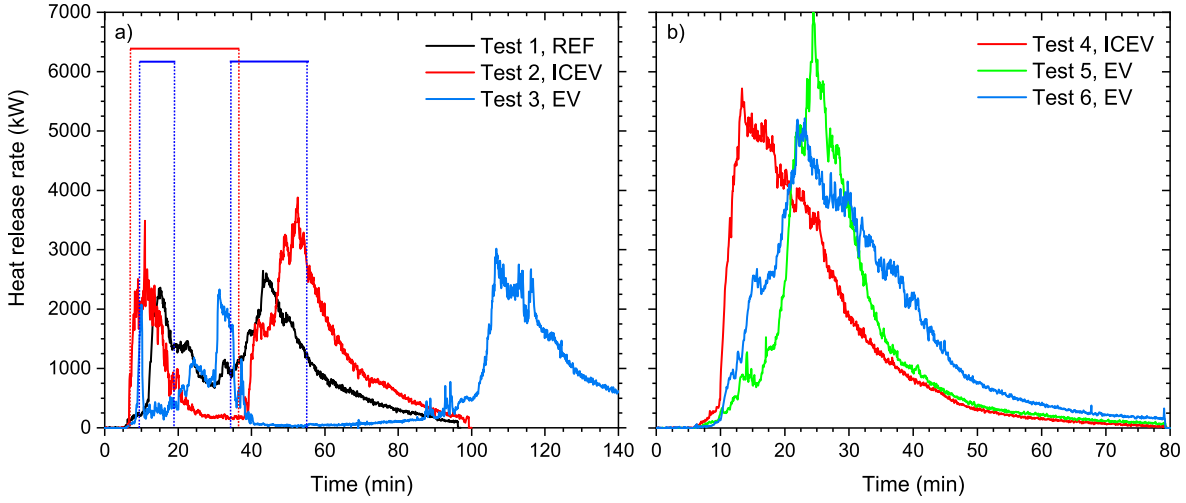

Fig. 2. HRR for a) tests 1–3, sprinkler active period for tests 2 and 3 are presented within the dotted lines and b) for tests 4–6 [17]. EVs in blue (tests 3 and 6) are prismatic cells and in green (test 5) are pouch cells. Fire ignition was performed at t = 5 min for all tests. (For interpretation of the references to colour in this figure legend, the reader is referred to the Web version of this article.)

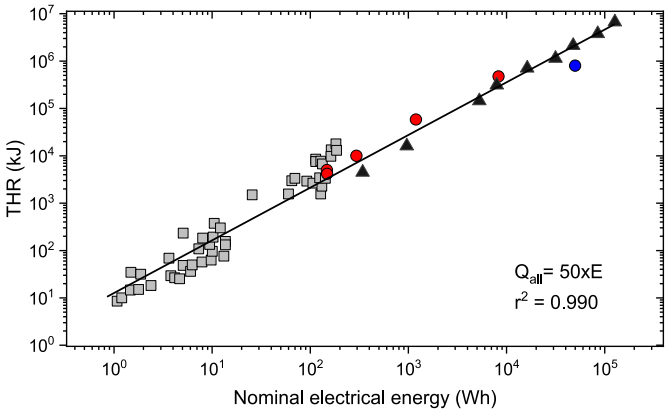

Fig. 3. THR plotted with respect to the nominal electrical energy (Q) for the test objects. Grey indicates cell/array tests, black are module/pack tests, red are cell/module tests from 2020 and blue is from the pack test in 2022. The black solid line indicates the linear fit for all data points. Note that logarithmic scales are used. (For interpretation of the references to colour in this figure legend, the reader is referred to the Web version of this article.)

somewhat higher than for the EV (test 3, Fig. 4b). The reason for the increased concentration of PAHs might be a result of the combustion of petrol. The sprinkler system was active during the time when the petrol was burning. Water application will lower the surrounding air temperature, which may result in a higher degree of incomplete combustion. Incomplete combustion of organic hydrocarbons was also noticed in the THC analysis. Here, the THC concentration was increased by a factor of two (for tests 2 and 3), compared to the free burning reference test (test 1). In addition, having an active sprinkler system reduced the total amount of soot in the combustion gases by ~50%. For test 5 (EV), the PAH concentration was much lower than for the remaining tests. Both for the particulate-bound PAHs and for PAHs in the gas phase; the reason for this discrepancy is unknown.

3.2.2. Analysis of CO_2 and CO

Looking at tests 2 and 3 (SUV) as well as tests 4 and 5 (van) (Fig. 4) it is evident that the total quantity of CO_2 and CO depends on the size/mass of the vehicle but not on the type of traction energy (i.e., if it is an EV or ICEV). The normalized quantity of CO_2 was marginally lower for the tests with the active sprinkler system (tests 2 and 3) compared to the free burning test of the same car model (test 1). However, the normalized amount of CO was similar for all three tests performed in 2022 (tests 1–3).

3.2.3. Particulate-bound metals and ions

The total quantity of metals and anions from the soot analysis is presented in Fig. 5. The quantity of particulate-bound metals is considerably higher for EVs compared to the ICEVs, in particular for the LIB specific elements: lithium, aluminium, cobalt, manganese and nickel.

Lead was found in higher quantities for the ICEVs, 7 and 18 g for tests 2 and 4, respectively, compared to 2.5–5 g for the EVs (tests 3, 5 and 6).

3.2.4. Hydrogen halides

For the tests performed in 2020 (tests 4–6), without a sprinkler system, HF differed the most between the ICEV (test 4) and the EVs (tests 5 and 6), see Fig. 6a. For the EV tested in 2022 (test 3), where water was applied, the HF concentration was significantly lower than for the EVs tested in 2020. In the period when the sprinkler system was active, no HF could be detected using FTIR see Fig. 6b. This was also the case for the battery pack test performed in 2022, see further Supplementary Material Fig. S2. However, analysis of the extinguishing water, filters, and impinger sampling confirmed the presence of fluoride ions (Supplementary Material Table S3).

In Fig. 7 the total amount of HX (HF, HCl and HBr) from the gas measurements is presented, which includes FTIR and the FTIR pre-filter, in comparison with the impinger sampling. Note that impinger sampling and FTIR pre-filters are analysed for ions (F^-, Cl^-, Br^-) and not for the acids (HCl, HF, HBr). The impinger sampling method is very sensitive and losses can be avoided to a higher degree compared to FTIR. It is expected that the concentrations obtained by analysing the gas-washing bottle liquid would be higher than those obtained using the FTIR, as the former possibly contain other water-soluble fluorides, chlorides and bromides in addition to HF, HCl and HBr.

However, for comparison, the amount of fluoride, chloride and bromide captured by the gas washing bottles and in the FTIR pre-filters

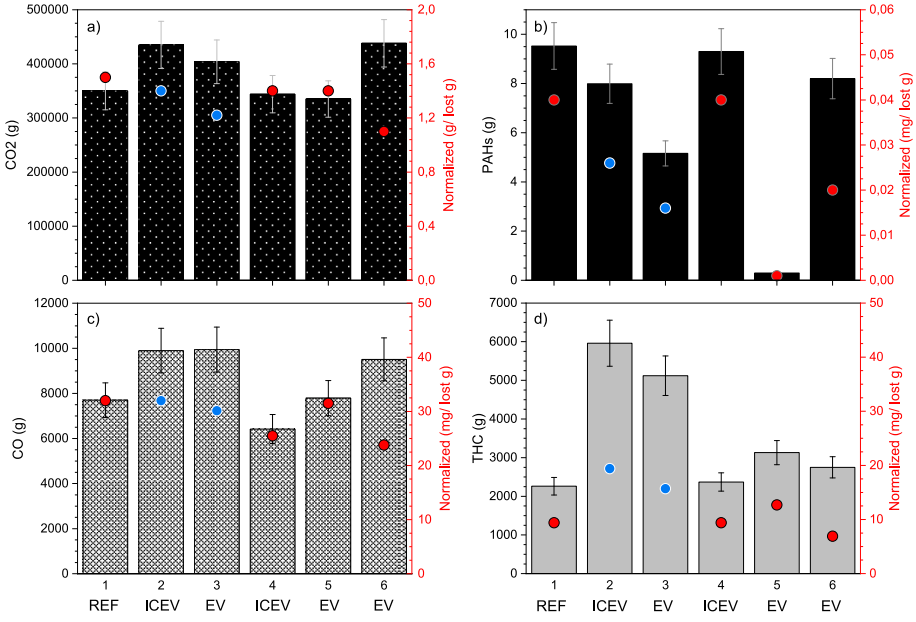

Fig. 4. Total quantity of a) CO_2, b) PAHs, c) CO and d) THC for each test. Note that water was applied using a sprinkler system in tests 2 and 3 (blue circles). Red and blue circles indicate the normalized amount i.e., the total quantity (in g or mg) divided with the total mass loss (in g) of the vehicle. (For interpretation of the references to colour in this figure legend, the reader is referred to the Web version of this article.)

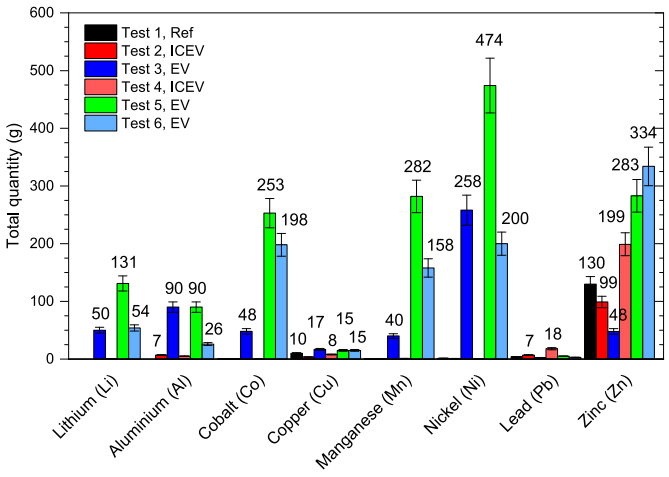

Fig. 5. Total quantities of particulate-bound metals and anions for each test.

were recalculated to HF, HCl and HBr. These extrapolations will likely lead to an overestimate of the concentration of HX. The total amount of HF ranged between 11 and 15 g for the tested ICEVs, and 120–859 g for the tested EVs.

3.3. HF concentrations from cells to vehicles

The total quantity of HF detected by the FTIR (including F^- in the pre-filter) plotted against the nominal electrical energy is presented in Fig. 8. Tests in 2020 were performed on the same type of battery cells but at different scales, from single cell to pack level. The production of HF is linearly proportional to the nominal electrical energy. For single cell tests, the only quantifiable gases detected by FTIR, in addition to HF, were CO and CO_2. Production of CO_2 is also linear, while production of CO is not. The larger the battery, the less efficient combustion, resulting in higher CO production.

Note that the tested cells were not enclosed; this means that losses of gas components/particles to the enclosure walls, i.e., "wall losses", are prevented. Increased "wall losses" could be a possible explanation why the measured HF quantities from EV fires are typically lower than for cell level tests as seen in Fig. 8.

4. Conclusions

Analysis of the combined results for HRR and emission measurements from the large-scale vehicle fire tests performed in this work confirm trends obtained from previous studies on EV and LIB fires [17]. Results regarding the burning behaviour, HRR, THR and peak HRR of EVs compared to ICEVs is critical for fire safety engineering. The peak HRR and THR were affected by the fire scenario and vehicle model (size of vehicle) but not significantly by the type of traction energy. The time to peak HRR was the shortest for the ICEVs, due to the release of a large

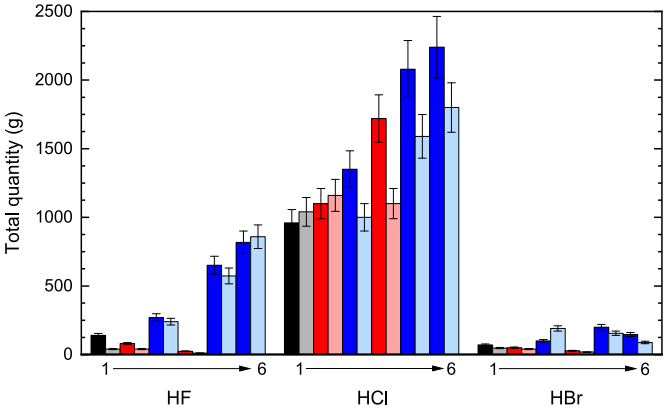

Fig. 7. Total quantity of HX for all tests, darker colours indicate impinger sampling and lighter shading FTIR. Reference test results in black/grey, ICEVs in red and EVs in blue. (For interpretation of the references to colour in this figure legend, the reader is referred to the Web version of this article.)

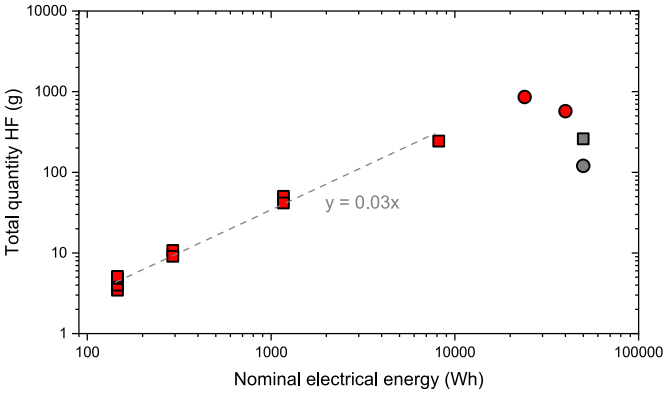

Fig. 8. HF quantity plotted with respect to the nominal electrical energy for the test objects. Red indicates tests performed in 2020, on single cells to pack level (squares) and EV tests (circles). Grey are tests performed in 2022, EV (circle) and battery pack (square). The grey dotted line shows the linear fit for the single cells to pack test series. Note that logarithmic scales are used. (For interpretation of the references to colour in this figure legend, the reader is referred to the Web version of this article.)

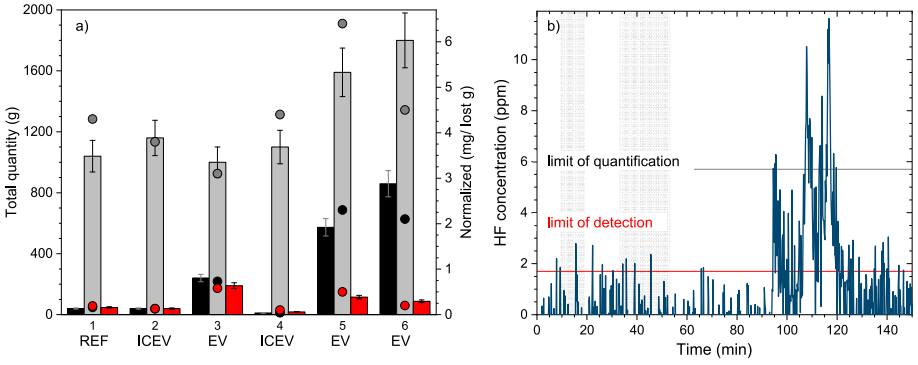

Fig. 6. a) Total quantity of HX measured using FTIR (including the FTIR pre-filter); black – HF, grey – HCl and red – HBr. Circles indicate the normalized amount of HX, HX (in mg) divided by the mass loss of the vehicle (in g). b) FTIR graph for test 3; blue shading indicates the time when the sprinkler system was active. (For interpretation of the references to colour in this figure legend, the reader is referred to the Web version of this article.)

amount of chemical energy when the fuel tank burst.

Regarding gas production, the total quantity of the gases measured were in the lower part or slightly below the quantities previously reported, especially for NO_x, HF and HCl. A higher concentration of lead was found for the tested ICEVs compared to the EVs, 7–18 g and 2.5–5 g, respectively. The ICEVs and EVs had similar lead-acid starter batteries.

HF, together with some specific battery metals such as nickel, cobalt, lithium and manganese (dependent on the cell chemistry), constituted the largest difference in the combustion gases between EVs and ICEVs. For the tested ICEVs, 11–15 g of HF was found, whereas the HF concentration for the EVs was between 120 and 859 g. Furthermore, when water was applied using the sprinkler system, quantification of HF using FTIR was inhibited. However, fluoride ions were detected in the FTIR pre-filters, impinger sampling and in the extinguishing water, indicating that fluoride containing species were released from the battery during this time. The variation in the reported concentrations of HF found in literature is vast, even for cell level tests. There could be several reasons for this large discrepancy. Firstly, the origin and amount of fluoride ions that can be released from a battery cell differ, and secondly, HF could readily react upon contact with other materials, which could lead to significant “wall losses”. Additionally, the extrapolation of data using fluoride ions to calculate HF concentrations will likely lead to an overestimation of the HF concentration. To be able to quantify HF, the origin of the fluoride ions in the filter sampling and impinger sampling should be further investigated. Furthermore, the analysed compounds presented in this study are only representative for a small number of tests. As vehicle type, battery chemistry, fire scenario etc. are varied, the gaseous compounds and concentrations of these will be subjected to variations.

Author statement

Jonna Hynynen: Project administration, conceptualization, experimental project leader, analysis of collected data, writing - original draft, review & editing. Ola Willstrand: Conceptualization, methodology, funding acquisition, review and editing. Per Blomqvist: Chemical analysis, review & editing. Petra Andersson: review and editing.

Funding

This work was supported by the Swedish Energy Agency [grant no. 48193-1, 48193-2].

Declaration of competing interest

The authors declare that they have no known competing financial interests or personal relationships that could have appeared to influence the work reported in this paper.

Data availability

Data can be made availiable upon request for non-commercial use

Acknowledgements

We would like to thank our colleagues at RISE as well as the following project partners: The Swedish Civil Contingencies Agency, If Skadeförsäkring, Länsförsäkringar Älvsborg, Länsförsäkringar Göteborg & Bohuslän, Stena Teknik, ColdCut systems, Borås Bildemontering, and the following fire and rescue services; Räddningstjänsten Storgöteborg, Södra Älvsborgs Räddningstjänstförbund, Storstockholms brandförsvar, Södertörns brandförsvarsförbund, Räddningstjänsten Luleå, Räddningstjänsten Syd. The car manufacturers providing the vehicles to the tests are greatly acknowledged.

Appendix A. Supplementary data

Supplementary data to this article can be found online at https://doi.org/10.1016/j.firesaf.2023.103829.

References

[1] R. Bisschop, O. Willstrand, F. Amon, M. Rosengren, Fire safety of lithium-ion batteries in road vehicles, RISE Rep. 50 (2019) 1–106. http://urn.kb.se/resolve?urn=urn:nbn:se:ri:diva-38873.
[2] P. Sun, R. Bisschop, H. Niu, X. Huang, A review of battery fires in electric vehicles, Fire Technol. 56 (2020) 1361–1410, https://doi.org/10.1007/s10694-019-00944-3.
[3] U. Bergholm, MSB PM - Sammanställning Av Bränder I Elfordon Och Eltransportmedel 2018–2020, Karlstad, 2021. https://rib.msb.se/filer/pdf/29438.pdf. (Accessed 20 March 2023).
[4] A.W. Brandt, K. Glansberg, Charging of electric cars in parking garages, RISE Rep. 30 (2020) (2020) 1–30. https://risefr.no/media/publikasjoner/upload/2020/report-2020-30-charging-of-electric-cars-in-parking-garages.pdf. (Accessed 1 July 2022).
[5] A. Rensmo, Per- and Polyfluoroalkyl Substances (PFAS) Emissions from Recycling Processes of Lithium-Ion Batteries, 2022. http://urn.kb.se/resolve?urn=urn:nbn:se:uu:diva-479345. (Accessed 4 July 2022).
[6] M. Wang, Q. Tan, L. Liu, J. Li, A facile, environmentally friendly, and low-temperature approach for decomposition of polyvinylidene fluoride from the cathode electrode of spent lithium-ion batteries, ACS Sustain. Chem. Eng. 7 (2019) 12799–12806, https://doi.org/10.1021/acssuschemeng.9b01546.
[7] P. Danz, V. Aryan, E. Möhle, N. Nowara, Experimental study on fluorine release from photovoltaic backsheet materials containing PVF and PVDF during pyrolysis and incineration in a technical lab-scale reactor at various temperatures, Toxics 7 (2019) 47, https://doi.org/10.3390/toxics7030047.
[8] H. Wingfors, R. Magnusson, L. Thors, M. Thunell, Gasformig HF vid brand i trånga utrymmen-risker för hudupptag vid insatser. https://rib.msb.se/filer/pdf/29507.pdf, 2021. (Accessed 12 January 2023).
[9] K. Dennerlein, F. Kiesewetter, S. Kilo, T. Jäger, T. Göen, G. Korinth, H. Drexler, Dermal absorption and skin damage following hydrofluoric acid exposure in an ex vivo human skin model, Toxicol. Lett. 248 (2016) 25–33, https://doi.org/10.1016/j.toxlet.2016.02.015.
[10] AISAB, Prehospital förmåga vid insatser med bränder i litiumjonbatterier. https://www.youtube.com/watch?v=vaspu8f_X_w, 2021. (Accessed 12 January 2023).
[11] F. Larsson, P. Andersson, P. Blomqvist, B.-E. Mellander, Toxic fluoride gas emissions from lithium-ion battery fires, Sci. Rep. 7 (2017), 10018, https://doi.org/10.1038/s41598-017-09784-z.
[12] P. Ribière, S. Grugeon, M. Morcrette, S. Boyanov, S. Laruelle, G. Marlair, Investigation on the fire-induced hazards of Li-ion battery cells by fire calorimetry, Energy Environ. Sci. 5 (2012) 5271–5280, https://doi.org/10.1039/C1EE02218K.
[13] L.D. Mellert, U. Welte, M. Hermann, M. Kompatscher, X. Ponticq, V. Hagerbach, Electric mobility and road tunnel safety hazards of electric vehicle fires. https://amberggroup.com/fileadmin/user_upload/news/Road_tunnel_safety_Hazards_of_electric_vehicle_fires_Mellert_2018.pdf, 2018. (Accessed 12 January 2023).
[14] DNV GL AS Maritime, Technical Reference for Li-Ion Battery Explosion Risk and Fire Suppression, Høvik, 2019. https://www.dnv.com/Publications/technical-reference-for-li-ion-battery-explosion-risk-and-fire-suppression-165062. (Accessed 26 January 2023).
[15] U. Bergström, Å. Gustafsson, L. Hägglund, C. Lejon, D. Sturk, T. Tengel, Screening of vented gases and aerosols from Li-ion LFP & NMC batteries under nitrogen atmosphere. https://www.msb.se/siteassets/dokument/publikationer/english-publications/vented-gases-and-aerosol-of-automotive-li-ion-lfp-and-nmc-batteries-in-humidified-nitrogen-under-thermal-load.pdf, 2015. (Accessed 26 January 2023).
[16] D. Sturk, L. Rosell, P. Blomqvist, A. Ahlberg Tidblad, Analysis of Li-ion battery gases vented in an inert atmosphere thermal test chamber, Batteries (2019) 5, https://doi.org/10.3390/batteries5030061.
[17] O. Willstrand, R. Bisschop, P. Blomqvist, A. Temple, J. Anderson, Toxic gases from fire in electric vehicles, RISE Rep. 90 (2020). http://urn.kb.se/resolve?urn=urn:nbn:se:ri:diva-52000.
[18] Å. Viklund, J. Björnstig, M. Larsson, U. Björnstig, car crash fatalities associated with fire in Sweden, Traffic Inj. Prev. 14 (2013) 823–827, https://doi.org/10.1080/15389588.2013.777956.
[19] L.D. Mellert, U. Welte, M. Tuchschmid, M. Held, M. Hermann, M. Kompatscher, M. Tesson, L. Nachef, Risk minimisation of electric vehicle fires in underground traffic infrastructures. https://plus.empa.ch/images/2020-08-17_Brandversuch-Elektroauto/AGT_2018_006_EMob_RiskMin_Undergr_Infrastr_Final_Report_V1.0.pdf, 2020. (Accessed 24 October 2022).
[20] A. Lönnermark, P. Blomqvist, Emissions from an automobile fire, Chemosphere 62 (2006) 1043–1056, https://doi.org/10.1016/j.chemosphere.2005.05.002.
[21] P.E. Schwarze, J. Øvrevik, M. Låg, M. Refsnes, P. Nafstad, R.B. Hetland, E. Dybing, Particulate matter properties and health effects: consistency of epidemiological and toxicological studies, Hum. Exp. Toxicol. 25 (2006) 559–579, https://doi.org/10.1177/096032706072520.
[22] C.A. Pope, D.W. Dockery, J. Schwartz, Review of epidemiological evidence of health effects of particulate air pollution, Inhal. Toxicol. 7 (1995) 1–18, https://doi.org/10.3109/08958379509014267.

[23] A. Seaton, D. Godden, W. MacNee, K. Donaldson, Particulate air pollution and acute health effects, Lancet 345 (1995) 176–178, https://doi.org/10.1016/S0140-6736(95)90173-6.
[24] K.W. Fent, D.E. Evans, Assessing the risk to firefighters from chemical vapors and gases during vehicle fire suppression, J. Environ. Monit. 13 (2011) 536, https://doi.org/10.1039/c0em00591f.
[25] J.L.A. Keir, U.S. Akhtar, D.M.J. Matschke, P.A. White, T.L. Kirkham, H.M. Chan, J. M. Blais, Polycyclic aromatic hydrocarbon (PAH) and metal contamination of air and surfaces exposed to combustion emissions during emergency fire suppression: implications for firefighters' exposures, Sci. Total Environ. 698 (2020), 134211, https://doi.org/10.1016/J.SCITOTENV.2019.134211.
[26] J.L.A. Keir, U.S. Akhtar, D.M.J. Matschke, T.L. Kirkham, H.M. Chan, P. Ayotte, P. A. White, J.M. Blais, Elevated exposures to polycyclic aromatic hydrocarbons and other organic mutagens in ottawa firefighters participating in emergency, on-shift fire suppression, Environ. Sci. Technol. 51 (2017) 12745–12755, https://doi.org/10.1021/acs.est.7b02850.
[27] C.S. Baxter, J.D. Hoffman, M.J. Knipp, T. Reponen, E.N. Haynes, Exposure of firefighters to particulates and polycyclic aromatic hydrocarbons, J. Occup. Environ. Hyg. 11 (2014), https://doi.org/10.1080/15459624.2014.890286. D85–D91.
[28] A. Lecocq, M. Bertana, B. Truchot, G. Marlair, Comparison of the fire consequences of an electric vehicle and an internal combustion engine vehicle, in: International Conference on Fires in Vehicles - FIVE 2012, Chicago, 2012, pp. 183–194. https://hal-ineris.archives-ouvertes.fr/ineris-00973680/document. (Accessed 12 January 2023).
[29] F. Larsson, P. Andersson, P. Blomqvist, A. Lorén, B.-E. Mellander, Characteristics of lithium-ion batteries during fire tests, J. Power Sources 271 (2014) 414–420, https://doi.org/10.1016/j.jpowsour.2014.08.027.
[30] D. Sturk, L. Hoffmann, A. Ahlberg Tidblad, Fire tests on E-vehicle battery cells and packs, Traffic Inj. Prev. 16 (2015) S159–S164, https://doi.org/10.1080/15389588.2015.1015117.
[31] A.W. Golubkov, S. Scheikl, R. Planteu, G. Voitic, H. Wiltsche, C. Stangl, G. Fauler, A. Thaler, V. Hacker, Thermal runaway of commercial 18650 Li-ion batteries with LFP and NCA cathodes – impact of state of charge and overcharge, RSC Adv. 5 (2015) 57171–57186, https://doi.org/10.1039/C5RA05897J.
[32] A.R. Baird, E.J. Archibald, K.C. Marr, O.A. Ezekoye, Explosion hazards from lithium-ion battery vent gas, J. Power Sources 446 (2020), 227257, https://doi.org/10.1016/j.jpowsour.2019.227257.
[33] B. Truchot, F. Fouillen, S. Collet, An experimental evaluation of toxic gas emissions from vehicle fires, Fire Saf. J. 97 (2018) 111–118, https://doi.org/10.1016/J.FIRESAF.2017.12.002.
[34] C. Lam, D. MacNeil, R. Kroeker, G. Lougheed, G. Lalime, Full-scale fire testing of electric and internal combustion engine vehicles, in: P. Andersson, B. Sundström (Eds.), Fires in Vehicles - FIVE 2016, Baltimore, 2016, pp. 95–106. https://ri.diva-portal.org/smash/get/diva2:1120218/FULLTEXT01.pdf. (Accessed 12 January 2023).
[35] N. Watanabe, O. Sugawa, T. Suwa, Y. Ogawa, M. Hiramatsu, H. Tomonori, H. Miyamoto, K. Okamoto, M. Honma, Comparison of fire behaviors of an electric-battery-powered vehicle and gasoline-powered vehicle in a real-scale fire test, in: P. Andersson, B. Sundström (Eds.), Fires in Vehicles - FIVE 2016, SP, Borås, 2016, pp. 195–206. http://urn.kb.se/resolve?urn=urn:nbn:se:ri:diva-30071.
[36] P. Sturm, P. Fößleitner, D. Fruhwirt, R. Galler, R. Wenighofer, S.F. Heindl, S. Krausbar, O. Heger, Fire tests with lithium-ion battery electric vehicles in road tunnels, Fire Saf. J. 134 (2022), 103695, https://doi.org/10.1016/j.firesaf.2022.103695.
[37] M. Quant, O. Willstrand, T. Mallin, J. Hynynen, Ecotoxicity evaluation of fire-extinguishing water from large-scale battery and battery electric vehicle fire tests, Environ. Sci. Technol. (2023), https://doi.org/10.1021/acs.est.2c08581.
[38] M. Dahlberg, The SP industry calorimeter. For rate of heat release measurements up to 10 MW, RISE Rep. 43 (1992) 1–22. http://urn.kb.se/resolve?urn=urn:nbn:se:ri:diva-4146.
[39] R.E. Lyon, R.N. Walters, Energetics of lithium ion battery failure, J. Hazard Mater. 318 (2016) 164–172, https://doi.org/10.1016/j.jhazmat.2016.06.047.
[40] A.O. Said, C. Lee, X. Liu, Z. Wu, S.I. Stoliarov, Simultaneous measurement of multiple thermal hazards associated with a failure of prismatic lithium ion battery, Proc. Combust. Inst. 37 (2019) 4173–4180, https://doi.org/10.1016/j.proci.2018.05.066.
[41] M. Chen, D. Zhou, X. Chen, W. Zhang, J. Liu, R. Yuen, J. Wang, Investigation on the thermal hazards of 18650 lithium ion batteries by fire calorimeter, J. Therm. Anal. Calorim. 122 (2015) 755–763, https://doi.org/10.1007/s10973-015-4751-5.
[42] X. Liu, S.I. Stoliarov, M. Denlinger, A. Masias, K. Snyder, Comprehensive calorimetry of the thermally-induced failure of a lithium ion battery, J. Power Sources 280 (2015) 516–525, https://doi.org/10.1016/j.jpowsour.2015.01.125.
[43] Y. Fu, S. Lu, K. Li, C. Liu, X. Cheng, H. Zhang, An experimental study on burning behaviors of 18650 lithium ion batteries using a cone calorimeter, J. Power Sources 273 (2015) 216–222, https://doi.org/10.1016/j.jpowsour.2014.09.039.
[44] P. Ping, D. Kong, J. Zhang, R. Wen, J. Wen, Characterization of behaviour and hazards of fire and deflagration for high-energy Li-ion cells by over-heating, J. Power Sources 398 (2018) 55–66, https://doi.org/10.1016/j.jpowsour.2018.07.044.
[45] D. Sturk, L. Hoffmann, A. Ahlberg Tidblad, Fire tests on E-vehicle battery cells and packs, Traffic Inj. Prev. 16 (2015) S159, https://doi.org/10.1080/15389588.2015.1015117. –S164.
[46] F. Larsson, P. Andersson, P. Blomqvist, B.-E. Mellander, Toxic fluoride gas emissions from lithium-ion battery fires, Sci. Rep. 7 (2017), 10018, https://doi.org/10.1038/s41598-017-09784-z.
[47] F. Larsson, P. Andersson, B.-E. Mellander, Lithium-ion battery aspects on fires in electrified vehicles on the basis of experimental abuse tests, Batteries 2 (2016), https://doi.org/10.3390/batteries2020009.
[48] P. Ping, Q. Wang, P. Huang, K. Li, J. Sun, D. Kong, C. Chen, Study of the fire behavior of high-energy lithium-ion batteries with full-scale burning test, J. Power Sources 285 (2015) 80–89, https://doi.org/10.1016/j.jpowsour.2015.03.035.
[49] Z. Wang, H. Yang, Y. Li, G. Wang, J. Wang, Thermal runaway and fire behaviors of large-scale lithium ion batteries with different heating methods, J. Hazard Mater. 379 (2019), 120730, https://doi.org/10.1016/j.jhazmat.2019.06.007.
[50] T.R. Long, A.F. Blum, T.J. Bress, B.R.T. Cotts, Best practices for emergency response to incidents involving electric vehicles battery hazards: a report on full-scale testing results, 2013, pp. 1–233. https://www.energy.gov/sites/prod/files/2014/02/f8/final_report_nfpa.pdf. (Accessed 18 January 2022).
[51] T.R. Long, A.M. Misera, Sprinkler protection guidance for lithium-ion based energy storage systems, in: Report number FPRF-2019-06-REV, 2019, pp. 1–46. https://www.nfpa.org//-/media/Files/News-and-Research/Fire-statistics-and-reports/Suppression/RFESSSprinklerProtection.pdf. (Accessed 22 March 2023).